# Simultaneous Excitation Systems for Ultrasonic Indoor Positioning

M. O. Khyam, Md. Noor-A-Rahim, Xinde Li, *Senior Member, IEEE*, Aruna Jayasuriya, Md. Apel Mahmud, *Senior Member, IEEE*, Amanullah M. T. Oo, *Senior Member, IEEE*, and Shuzhi Sam GE, *Fellow, IEEE*

***Abstract*—Ultrasonic technology is a tool in the area of indoor positioning systems (IPSs) and has been extensively used in many applications. In ultrasonic IPSs (UIPSs), the use of a chirp signal (in which the frequency varies with time) is widespread due to its capability to obtain high-range resolution through its time-frequency characteristic. It also provides an opportunity to design effective waveform diversity which has always been the key to mitigating multiple-access interference (MAI) in multi-user UIPSs. To explore this, we analyze the chirp signal from the signal design perspective, with the goal of developing a precise and efficient UIPS for multi-user environments. To achieve this, three waveform diversity design schemes are proposed in which all the benefits of the classical chirp, such as high-range resolution, are retained while all the transmitters can transmit chirp signals simultaneously. In each scheme, a linear chirp is divided into two linear sub-chirps with diverse durations and/or bandwidths. This process is optimized by selecting the concatenated sub-chirps that generate a waveform which has a high-range resolution and relatively low interference in the same scheme. Initially, the effectiveness of the proposed schemes is evaluated for five simultaneous excitation signals using several metrics and experimental results are then presented for the ultrasonic indoor positioning.**

***Index Terms*—Chirp, waveform design, multiple-access interference, ultrasonic indoor positioning**

## I. Introduction

RECENTLY, a large number of stimulating new location-dependent applications, in which accurate information of the locations of the targets is a prerequisite, has appeared. Although a user's location can be obtained outdoors through a global positioning system (GPS), due to signal attenuation caused by a building's materials, it is unavailable in indoor environments where there is a large amount of human activity [1]. Therefore, during the last decade, significant efforts have been made towards designing a capable yet precise and low-cost indoor positioning system (IPS), with different types of indoor positioning technologies developed. IPSs are commonly divided into five categories: optical; mechanical; magnetic; radio frequency (RF); and ultrasound [2], [3]. Of them, ultrasonic IPSs (UIPSs) have been widely used since they are cost-effective yet precise and robust [4]. However, one of their fundamental problems is that they suffer from multiple-access interference (MAI) when multiple transmitters transmit ultrasonic signals simultaneously [5]. A common strategy for avoiding MAI in a UIPS is to transmit signals from an individual transmitter at different times with proper intervals using a time-division multiple access (TDMA) technique which reduces a system's update rate [6]. One of the strategies for minimizing MAI in a UIPS is to assign each transmitter a unique waveform in such a way that, at the receiving end, they can be effectively separated after pulse compression. Attempts to mitigate MAI have generally relied on modulation schemes, such as the direct sequence spread spectrum (DSSS) [7], [8], frequency hopping spread spectrum (FHSS) [7], [8], code division multiple-access (CDMA) [3], [9], [10], orthogonal frequency division multiple-access (OFDMA) [11], [12], discrete multi-tone modulation [13], carrier sense multiple-access (CSMA) [14] and filter bank-based multi-carrier modulation [15]. In recent years, in the field of multiple-access UIPS, a chirp-based modulation scheme has gained popularity and attracted a great deal of attention not only for its capability to enhance range resolution through pulse compression (i.e., cross-correlation) but also its effective waveform diversity provided by its time-frequency characteristic [16]. As this paper focuses on chirp-based multiple-access ultrasonic positioning, here we only describe those which are related to the proposed scheme and a comprehensive review can be found in [3]. In [17], to minimize MAI in a chirp-based UIPS, four orthogonal sets of chirps, each of which contains three waveforms, are presented. The first set is generated by interconnecting two linear sub-chirps that change at the halfway point of the signal's duration. In this set, the first and second waveforms are generated in such a way that when the sub-chirps are concatenated, they respectively form linear up-chirp and linear down-chirps. In this scheme, to generate the third waveform, respectively, the first and second waveforms (i.e., the linear up- and down-chirps) are used as sub-chirps for the first half and second half of the signal duration. Within this scheme, a fourth waveform can be generated by interchanging the sub-chirps of the third waveform (i.e., by taking the time-reversal of the third waveform). Therefore, in this set, only four unique waveforms

This work was supported in part by the National Natural Science Foundation of China under Grant 61573097 and Grant 91748106, in part by the Key Laboratory of Integrated Automation of Process Industry under Grant PALN201704. (Corresponding author: M. O. Khyam.)

M. O. Khyam and Aruna Jayasuriya, are with the School of Engineering and Technology, Central Queensland University, Australia (email: m.khyam@cqu.edu.au and a.jayasuriya@cqu.edu.au).

Md Noor-A-Rahim is with School of Computer Science & IT, University College Cork, Cork, Ireland (email: m.rahim@cs.ucc.ie).

Xinde Li is with the Key Laboratory of Measurement and Control of CSE (School of Automation, Southeast University), Ministry of Education, Nanjing, China (e-mail: xindeli@seu.edu.cn).

Md. Apel Mahmud and Aman Maung Than Oo are with School of Engineering Deakin University, Geelong, VIC, Australia (email: apel.mahmud@deakin.edu.au, aman.m@deakin.edu.au).

Shuzhi Sam Ge is with the Social Robotics Laboratory, Interactive Digital Media Institute, Department of Electrical and Computer Engineering, National University of Singapore, Singapore 117576 (e-mail:samge@nus.edu.sg).

can be generated. The second set of [17] also decomposes each chirp into two interconnected sub-chirps but with different frequency rates that change at the halfway point of the signal's duration. Thus, in this scheme, it is possible to generate a large number of unique chirp waveforms, as shown in [18]. The detailed description of this set is given at the end of this section, as well as in Section II. The third set of [17] uses chirp rates of a nonlinear chirp, particularly, trigonometric (sine and cosine) chirps, as a mechanism for assigning uniquely modulated chirp signals to transmitters. In set 4, the OFDM principle is combined with a chirp waveform, i.e, it interleaves zeros between the discrete frequency components of a chirp waveform and the data sequence is then shifted to generate multiple orthogonal chirp signals. The major problem of sets 3 and 4 is that they suffer from ambiguities. It is important to note that, of these sets, set 2 (also used in [16], which was adopted from wireless data communication [19]), can be considered the most promising multiple-access technique since it enables the generation of a large number of unique chirp waveforms. For ease of discussion and representation, we call this set as a conventional technique throughout this paper. The time-frequency diagram of this technique is shown in Fig. 1(a) in which it is clear that, when the number of transmitters in the system is increased, not only does the similarity between successive chirps increase (which degrades the cross-correlation's performance) but also the chirp rate of either the first or second interconnected chirp decreases which causes the auto-correlation's performance to deteriorate (details are provided in Section IV). Therefore, to enhance the target detection performance achieved in [16], [19] in a multiple-access environment, its auto- and cross-correlation performances should be further improved.

In this paper, initially, the reason for the low correlation performance of the conventional design [16], [19] is investigated and then three waveform diversity design schemes proposed to improve this situation. In each scheme, the duration and/or bandwidth is assumed to be diverse and designed specially to generate a waveform with impulse-like auto-correlation and relatively flat cross-correlations to the other waveforms available in the scheme.

The remaining sections of this paper are organized as follows. Section II illustrates the signal model of a conventional design scheme and the new waveform design schemes are presented in Section III. In Section IV, for the conventional and proposed methods, firstly, examples of their designs are discussed and then correlation analyses conducted. The experimental procedure for determining the accuracy of each of the proposed design schemes for a UIPS is discussed in Section V and the results obtained presented in Section VI. Finally, the conclusions of this work are drawn in Section VII.

## II. Signal Model of Chirp-based Multiple-access Scheme

In the proposed ultrasonic multiple-access scheme, each transmitted chirp is constructed from two linear sub-chirps, each with characteristics of a non-overlapping frequency and full bandwidth usage. It is considered that a UIPS has $M$ transmitters which simultaneously transmit a signal ($s_m(t),\ m = 1,\ 2, \cdots, M$) with a duration of $T$ and bandwidth of $B = f_{\max} - f_{\min}$ (where $f_{\min}$ and $f_{\max}$, respectively, represent the minimum/initial and maximum/final frequencies of the signal). As each waveform consists of two sub-chirps, let $t_{m1}$ & $t_{m2}$, $f_{m1}$ & $f_{m2}$, and $k_{m1}$ & $k_{m2}$, respectively, represent the durations, starting frequencies and chirp rates of the first and second sub-chirps of the $m$th signal. Now, the transmitted pulse of the $m$th transmitter is defined as:

$$s_m(t) = \begin{cases} \exp\left\{j2\pi\left(f_{m1}t + \frac{1}{2}k_{m1}t^2\right)\right\} & \text{for } 0 \le t < t_{m1} \\ \exp\left\{j2\pi\left(f_{m2}t + \frac{1}{2}k_{m2}t^2\right)\right\} & \text{for } t_{m1} \le t \le T \end{cases} \tag{1}$$

The corresponding durations, starting frequencies and chirp rates are defined, respectively, as:

$$\begin{aligned} t_{m1} &= \alpha(m)T \\ t_{m2} &= T - t_{m1} \\ f_{m1} &= f_{\min} \\ f_{m2} &= f_{\max} \\ k_{m1} &= \frac{B_1}{t_{m1}} \\ k_{m2} &= \frac{B_2}{T - t_{m1}} \end{aligned} \tag{2}$$

where $B_1$ and $B_2$ represent the bandwidths of the first and second sub-chirps, respectively, which can be defined as:

$$\begin{aligned} B_1 &= \xi(m)B \\ B_2 &= B - B_1 \end{aligned} \tag{3}$$

In equations (2) and (3), $0 \le \alpha(m) \le 1$ and $0 \le \xi(m) \le 1$ are the parameters for controlling the various durations and bandwidths of the waveforms, respectively. If $\alpha(m)$ and $\xi(m)$ are equal to 0 or 1, the corresponding waveform only contains a single segment.

The cross-correlation function (CCF) between the $u$th and $v$th transmitted waveforms is defined as [20]:

$$C_{u,v}(\tau) = \frac{1}{T} \cdot \begin{cases} \sum_{n=-T}^{n=-T+t_{u1}+t_{v2}} s_{u1}[n] \cdot s_{v2}[n-\tau] \\ -T \le \tau \le -T + t_{u1} + t_{v2} \\ \sum_{n=-T+t_{u1}}^{n=t_{v2}} s_{u2}[n] \cdot s_{v2}[n-\tau] \\ -T + t_{u1} \le \tau \le t_{v2} \\ \sum_{n=-T+t_{v2}}^{n=t_{u1}} s_{u1}[n] \cdot s_{v1}[n-\tau] \\ -T + t_{v2} \le \tau \le t_{u1} \\ \sum_{n=T-t_{u2}-t_{v1}}^{n=T} s_{u2}[n] \cdot s_{v1}[n-\tau] \\ T - t_{u2} - t_{v1} \le \tau \le T \end{cases} \tag{4}$$

where $s_{u(v)1}$ and $s_{u(v)2}$ represent the first and second segments of the $u$th and $v$th waveform, respectively. The basic concept of equation (4) is to perform cross-correlation between $s_{u(v)1}$ and $s_{u(v)2}$ of the $u$th and $v$th waveform in each time step. In this equation, one of the segments remains stationary, while the other one slide across over the stationary one, updating the information contained within the time frame. This equation will generate a maximum cross-correlation coefficient

This article has been accepted for publication in a future issue of this journal, but has not been fully edited. Content may change prior to final publication. Citation information: DOI 10.1109/JSEN.2020.3006930, IEEE Sensors Journal



if there is a match between the sub-chirps in a specific time step and in the case of a mismatch, it will result in low cross-correlation coefficients. This technique has extensively been used in simultaneous excitation systems to analyze the MAI.

If we set $u = v$ in equation (4), the auto-correlation function (ACF) of each transmitted waveform can be obtained as [20]:

$$C_m(\tau) = \frac{1}{T} \cdot \begin{cases} \sum_{\substack{n=-T \\ n=t_{m1}}}^{n=0} s_{m1}[n] \cdot s_{m2}[n-\tau] & -T \le \tau \le 0 \\ \sum_{\substack{n=-t_{m1} \\ n=-t_{m2}}} s_{m1}[n] \cdot s_{m1}[n-\tau] & -t_{m1} \le \tau \le t_{m1} \\ \sum_{\substack{n=-t_{m2} \\ n=T}} s_{m2}[n] \cdot s_{m2}[n-\tau] & -t_{m2} \le \tau \le t_{m2} \\ \sum_{n=0} s_{m2}[n] \cdot s_{m1}[n-\tau] & 0 \le \tau \le T \end{cases} \tag{5}$$

where the second and third terms are the ACFs of segments $s_{m1}$ and $s_{m2}$, respectively, which are the same as that of a single linear chirp, with the first and last terms the CCFs between $s_{m1}$ & $s_{m2}$ and $s_{m2}$ & $s_{m1}$, respectively.

As, in [16], [17], [19], it is proposed to set $\alpha(m) = 0.5$ and $\xi(m) = \frac{m}{M+1}$, equations (3) and (2) can be rewritten as:

$$\begin{aligned} B_1 &= \left(\tfrac{m}{M+1}\right) B \\ B_2 &= \left(\tfrac{m-M-1}{M+1}\right) B \end{aligned} \tag{6}$$

and

$$\begin{aligned} t_{m1} &= 0.5T \\ t_{m1} &= t_{m2} = 0.5T \\ f_{m1} &= f_{\min} \\ f_{m2} &= f_{\max} \\ k_{m1} &= \tfrac{mB}{0.5T(M+1)} \\ k_{m2} &= \tfrac{(m-M-1)B}{0.5T(M+1)} \end{aligned} \tag{7}$$

Therefore, in this conventional method (which is set 2 of [17]), when the number of transmitters ($M$) in the system is increased, as per equation (7): firstly, the chirp rate of either the first ($k_{m1}$) or second ($k_{m2}$) interconnected chirp decreases and one of the interconnected sub-chirps acts as an approximate single-tone signal for half the total duration; and secondly, the difference in chirp rates between the waveforms decreases. Equations (4) and (5) show that, in the time domain, two sub-chirps effectively slide across each other and generate a product vector comprising the sum of the products of the values currently aligned in each time step. Therefore, if a sub-chirp acts as an approximate single-tone signal and the difference in chirp rates between the waveforms decreases while sliding across during the correlation, the auto-correlation width (as per equation (5)) and cross-correlation value (as per equation (4)), respectively, will increase. Therefore, although the conventional method [16], [19] simplifies the chirp design procedure, this does not guarantee an optimum suppression of cross-correlation or the optimum width of auto-correlation. However, as the control parameters $\alpha$ and $\xi$ clearly provide an opportunity to improve the correlation properties of the waveforms, in the following section, three new design schemes are proposed.

## III. Proposed structures of waveforms for multiple access

Before designing the chirp waveforms which should provide better correlation properties, we first set the designs' objectives. For $M$ waveforms, a natural optimization is to respectively select a chirp waveform that produces an impulse-like auto-correlation (i.e., low side lobes and auto-correlation width) and relatively flat cross-correlation (i.e., low cross-correlation peak). Therefore, an objective function ($E$) for an excitation signal which minimizes the side lobes of the auto-correlation and peaks of the cross-correlations from the minimum distance formula is defined as:

$$E = \min_{\substack{u,v=1,2,\cdots,M,u\neq v \\ -T<\tau'<\frac{1}{B} \text{or} \frac{1}{B}<\tau'<T \\ -T<\tau<T}} \left( (\max(|C_{u,u}(\tau')|))^2 + (\max(|C_{u,v}(\tau)|))^2 \right) \tag{8}$$

where $C_{u,u}(\tau')$ and $C_{u,v}(\tau)$ are the ACF of the $u$th waveform and CCF of the $u$th and $v$th waveforms, respectively. We set the condition $-T < \tau' < \frac{1}{B} \text{or} \frac{1}{B} < \tau' < T$ because the side lobes of the auto-correlation always lie within this range whereas the main lobe is in the range of $-\frac{1}{B} < \tau' < \frac{1}{B}$.

Now, a minimum $E$ can be achieved by optimizing the duration ($t_{m1}$) and bandwidth ($B_1$) of the first sub-chirp using the control parameter $\alpha$ and $\xi$, respectively. To obtain the optimum $\alpha$ and $\xi$ for each waveform, in the following subsections, three optimization procedures are discussed.

### A. Bandwidth optimization

Let for $M$ excitation signals the control parameter is the bandwidth of the first sub-chirp ($\xi = [\xi(0), \xi(1), \cdots, \xi(M-1)]^\intercal$) and the duration of each sub-chirp is constant as per equation (7) (i.e, $\alpha$ = 0.5). Now, the optimum value of $\xi(m)$, based on the objective function $E$, is established as:

$$\begin{cases} \min\limits_{\substack{u,v=1,2,\cdots,M,u\neq v \\ -T<\tau'<\frac{1}{B} \text{or} \frac{1}{B}<\tau'<T \\ -T<\tau<T}} \left( (\max(|C_{u,u}(\tau')|))^2 + (\max(|C_{u,v}(\tau)|))^2 \right) \\ \text{such that} \\ 0 < \xi(m) < 1, m = 1, 2, \cdots, M \end{cases} \tag{9}$$

where the range of bandwidths of the first sub-chirp is confined by the constraint. The optimal bandwidth of the first sub-chirp of $M$ waveforms can be found by solving equation (9) and, based on these values, $M$ excitation signals with good correlation properties can be obtained. An example of this proposed bandwidth optimization scheme is executed for five excitation signals, with the results presented in the time-frequency diagram in Fig. 1(b).

This article has been accepted for publication in a future issue of this journal, but has not been fully edited. Content may change prior to final publication. Citation information: DOI 10.1109/JSEN.2020.3006930, IEEE Sensors Journal



### B. Time Optimization

As, apart from the various $\xi$ that control the bandwidth of the first sub-chirp, different $\alpha$ that control its duration can also minimize $E$, this is our second strategy. Let for $M$ excitation signals the control parameter is the duration of the first sub-chirp ($\alpha = [\alpha(0), \alpha(1), \cdots, \alpha(M-1)]^\intercal$) and bandwidth of the first sub-chirp maintained as per equation (6) (i.e, $\xi(m) = \frac{m}{M+1}$). Now, the optimum $\alpha(m)$ is established as follows based on the objective function $E$:

$$\begin{cases} \min\limits_{\substack{u,v=1,2,\cdots,M,u\neq v \\ -T<\tau'<\frac{1}{B}\text{or}\frac{1}{B}<\tau'<T \\ -T<\tau<T}} \left((\max(|C_{u,u}(\tau')|))^2 + (\max(|C_{u,v}(\tau)|))^2\right) \\ \text{such that} \\ \qquad 0 < \alpha(m) < 1, m = 1, 2, \cdots, M \end{cases} \tag{10}$$

where the range of duration values of the first sub-chirp is confined by the constraint. The optimal durations of the first sub-chirps of $M$ waveforms can be found by solving equation (10) and, based on these values, $M$ excitation signals with good correlation properties can be obtained. An example of this proposed time optimization scheme is executed for five excitation signals, with the results presented in the time-frequency diagram in Fig. 1(c).

### C. Joint Optimization

The idea behind this approach is to optimize both parameters ($\alpha$ and $\xi$) jointly as follows, instead of separately optimizing them:

$$\begin{cases} \min\limits_{\substack{u,v=1,2,\cdots,M,u\neq v \\ -T<\tau'<\frac{1}{B}\text{or}\frac{1}{B}<\tau'<T \\ -T<\tau<T}} \left(\max\left(|C_{u,u}(\tau')|\right)\right)^2 + \left(\max\left(|C_{u,v}(\tau)|\right)\right)^2 \\ \text{such that} \\ \qquad 0 < \alpha(m) < 1, m = 1, 2, \cdots, M \\ \qquad 0 < \xi(m) < 1, m = 1, 2, \cdots, M \end{cases} \tag{11}$$

where the range of duration values and bandwidths of the first sub-chirp first sub-chirp are confined by the constraints. The optimal durations and bandwidths of the first sub-chirp of $M$ waveforms can be found by solving equations (11) and, based on these values, $M$ excitation signals with good correlation properties can be obtained. n example of this proposed joint optimization scheme is executed for five excitation signals, with the results presented in the time-frequency diagram in Fig. 1(d). Please note that all the optimization models in equations (9) to (11) are constrained nonlinear problems [21] which can be solved by the sequential quadratic programming (SQP) solver available in Matlab.

## IV. Examples of Designs and Correlation Analyses

In this section, we present some examples of the designs of the proposed methods and a correlation analysis of each of them which is considered an effective tool for evaluating the MAI to UIPSs in a multiple-access environment. The simulation results obtained are compared with the conventional technique [16], [19]. For the performance evaluations, we use five (i.e., $m = 1, 2, \cdots, M$ with $M = 5$) 38-44 kHz/12 ms chirp signals (i.e., $f_{\text{min}}$ = 38 kHz, $f_{\text{max}}$ = 44 kHz, $B = f_{\text{max}} - f_{\text{min}}$= 6 kHz and $T$=12 ms) sampled at 1 MHz.

Now, based on the above parameters, we implement the conventional as well as our proposed schemes, with their time-frequency diagrams shown in Fig. 1. It can be seen that, unlike in Fig. 1(a), (the conventional scheme), for the proposed: (i) bandwidth optimization technique, in Fig. 1(b), the bandwidth of each sub-chirp is optimized as per equation (9) while the duration of the sub-carriers remains constant (the same as the conventional technique); (ii) time optimization technique, in Fig. 1(c), the duration of each sub-chirp is optimized as per equation (10) while the bandwidth of the sub-carriers remains the same as the conventional technique; and (iii) joint optimization technique, in Fig. 1(d), the duration and bandwidth of each sub-chirp is optimized as per equation (11). The numerical values of the control parameters ($\xi$ and $\alpha$) of the conventional and proposed design schemes are given in Table-I (i.e., the corresponding value of Fig. 1).

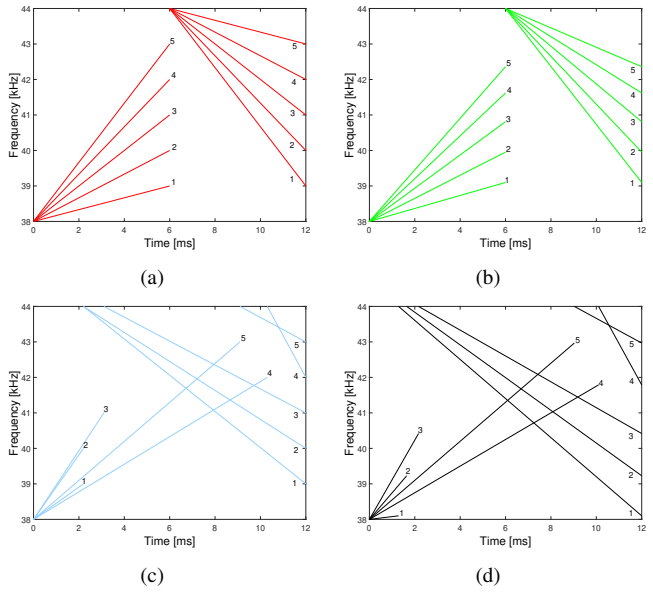


Fig. 1: Time-frequency diagram of 38–44 kHz/12 ms chirp for (a) conventional method [16], [19] (i.e, without optimization) and proposed (b) bandwidth optimization, (c) time optimization and (d) joint optimization techniques

The complexity of the proposed methods lies on the signal design which is a pre-processing step of any UIPS. Therefore, the complexity of the proposed method is the amount of time required to generate $M$ number of waveforms with impulse-like auto-correlations and relatively flat cross-correlations. In the proposed scheme, if $M$ is increased, the computational complexity is also increased. It is important to note that the time required for the joint optimization technique to generate $M$ number of waveforms is high when compared to the bandwidth and time optimization techniques. This is because the joint optimization technique requires to optimize two parameters (bandwidth and time), whereas the bandwidth and time optimization techniques need to optimize one parameter (either bandwidth or time).

This article has been accepted for publication in a future issue of this journal, but has not been fully edited. Content may change prior to final publication. Citation information: DOI 10.1109/JSEN.2020.3006930, IEEE Sensors Journal



TABLE I: Numerical values of the control parameters of the conventional and proposed design schemes

| Method | Transmitter index | $\xi$ | $\alpha$ |
|---|---|---|---|
| Conventional technique, Bandwidth optimization, Time optimization & Joint optimization | 1 | 0.1667,0.1830,0.1667,&0.0200 | 0.500,0.500,0.1092,&0.1050 |
| | 2 | 0.3333,0.7268,0.3333,&0.2000 | 0.500,0.500,0.1410,&0.1350 |
| | 3 | 0.5000,0.3257,0.5000,&0.4333 | 0.500,0.500,0.1410,&0.1833 |
| | 4 | 0.6667,0.4683,0.6667,&0.5983 | 0.500,0.500,0.8583,&0.8417 |
| | 5 | 0.8333,0.6033,0.8333,&0.8333 | 0.500,0.500,0.7583,&0.7500 |

To validate the effectiveness of the proposed methods, the correlation properties of the designed waveforms are analyzed and compared with the conventional method in Fig. 2. It is clear that the ACFs of the proposed time and joint optimization methods provide much narrower peaks than the conventional one (i.e., better range resolutions) while those of the proposed bandwidth optimization are almost the same. This is because, for the conventional and proposed bandwidth optimization methods, except of the one waveform (the third and fourth waveforms of the conventional and bandwidth optimization methods, respectively), as the chirp rate of either the first or second sub-chirp decreases (Fig. 1(a)), this sub-chirp acts as an approximate single-tone signal for half the total duration. Therefore, when the sub-chirps slide across each other during the auto-correlation operation, a larger auto-correlation width is generated. On the other hand, for the proposed time and joint optimization techniques, as none of the sub-chirps acts like a single-tone signal (at least for a longer period of time), the widths of the ACFs remain consistent for all the waveforms and are almost the same as that of the ACF of a linear chirp.

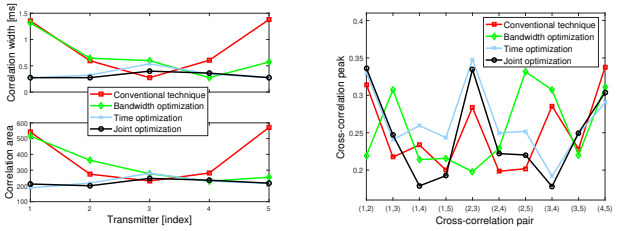


(a) (b)

Fig. 2: Comparisons of (a) auto-correlation's width and (b) maximum cross-correlation's value (between waveforms) of conventional and proposed designed schemes for five waveforms

It is observed that the auto-correlation performance of the joint optimization method is better than that of the frequency and time optimization techniques as, in the former, both the time and bandwidth are optimized. Note that the widths of the ACFs (Fig. 2(a)) are found using a threshold-based search mechanism. The threshold is set to 22% of the height of the ACF as this value guarantees a fair comparison of the ACFs between the linear chirp, conventional technique and proposed schemes. To further illustrate this phenomenon, for the worst-case scenario (i.e., when the width of the ACF in Fig. 2(a) is the maximum), the ACFs of the conventional and proposed methods are compared with that of a linear chirp in Fig. 3. Figs. 2(a) and 3 imply that the ACFs of the proposed methods (notably, the time and joint optimization ones) are comparable with that of a linear chirp (for the case of a single emission). In Fig. 2(b), it can be seen that the cross-correlation performances of the proposed methods and conventional waveforms are almost the same as, in all cases, the similarity between the waveforms in each scheme is the same but significantly low for a multiple-access environment. Please note that the

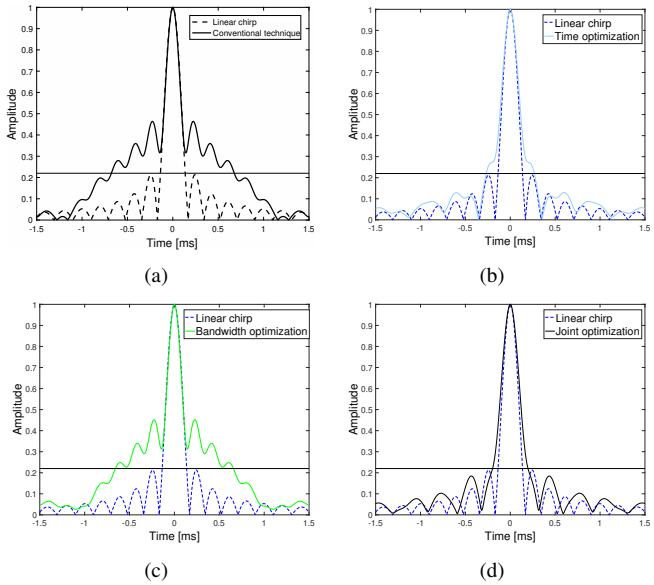


(a) (b) (c) (d)

Fig. 3: Comparisons of envelopes of auto-correlation between linear-chirp and (a) conventional method, (b) proposed bandwidth optimization, (c) proposed time optimization and (d) proposed joint optimization techniques (for worst-case scenario)

transmitters are used as a pattern for the correlation results (shown in Figs. 2 and 3). Although Fig. 2(b) shows the cross-correlation results between pairs of transmitters, which can be useful to know the pair that presents the worst cross-correlation, it does not correspond to a simultaneous emission of the five transmitters. Therefore, in Fig. 4, an analysis that includes the variation of the mainlobe to sidelobe ratio (MLSLR) with the number of emitters is presented. This figure shows that in a multiple-access environment when the number of transmitters is increased, the MLSLR is also increased for both conventional and proposed schemes. However, it is clear that the MLSLRs of the proposed time and joint optimization methods are lower than the conventional one, while those of the proposed bandwidth optimization is almost the same. The reason behind this phenomenon is that the width of the ACFs. When the widths of the ACFs are increased in a multiple-access environment, the MLSLRs are also increased (e.g., see Fig. 3). For the ease of clarity, the cross-correlation of the received signal (received by the central receiver, con-

This article has been accepted for publication in a future issue of this journal, but has not been fully edited. Content may change prior to final publication. Citation information: DOI 10.1109/JSEN.2020.3006930, IEEE Sensors Journal



sidering all five emitters operating simultaneously) with the code pattern of each transmitter is also shown in Fig. 5.

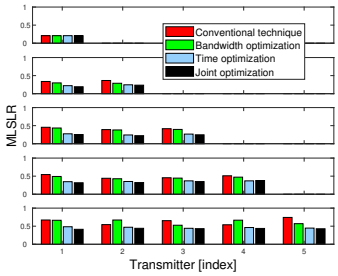


Fig. 4: MLSLR (from simulation results) when all transmitters operating simultaneously

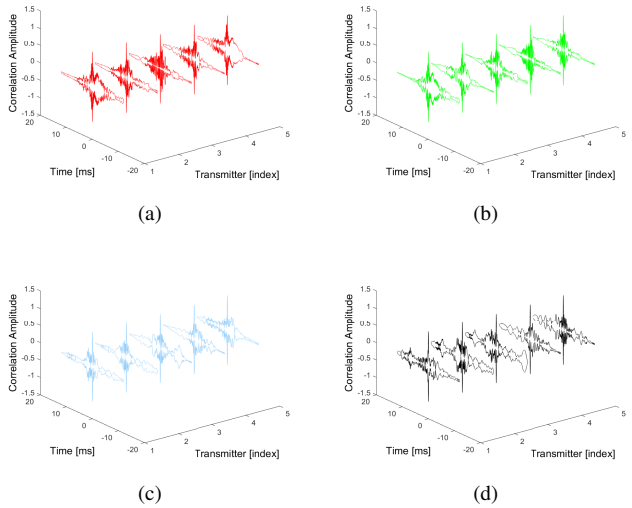


Fig. 5: Cross-correlation of the received signal considering all emitters operating simultaneously (from simulation results): (a) conventional method, (b) proposed bandwidth optimization, (c) proposed time optimization, and (d) proposed joint optimization techniques

Therefore, the effectiveness of the proposed design schemes is confirmed through correlation analyses which is then validated experimentally for a multiple-access UIPS, as discussed in the following section.

## V. System Architecture

The experimental arrangement of the proposed UIPS is shown in Fig. 6 and the illustration of the connection diagram between transmission and reception architectures of UIPS is shown in Fig. 7. In an active mobile architecture, nine ultrasonic Piezotite MA40S4R devices were placed as receivers (reference points) on a plane inside a room where, as the distance between the receivers was 30 cm, the dimension of the receiver plane was 60 cm $\times$ 60 cm. On the other hand, approximately 120 cm away from the receiver plane, as five ultrasonic Piezotite MA40S4S devices were placed on a single plane as transmitters, with the distance between them 15 cm, the dimension of the transmitter plane was 30 cm $\times$ 30 cm. Note that although these transducers allow detection of the signal at a maximum distance of 400 cm, our analysis is limited to a maximum of 120 cm for the proposed multiple-access system to ensure a better signal reception. In [17], it has been shown that when the distance between the transmitter and receiver is reached to approximately 400 cm, the signal reception becomes poor (for the same transducers). The transmitter plane was attached to a Vernier scale (the precision of which was 0.05 mm) and moved 10 cm in the $z$ direction with the aim of localizing the transmitters. To compare the quality parameters such as MLSLR between the simulation and experimental results, another experiment was conducted using the same setup where it was ensured that there was no multi-path in the environment and five transmitters were introduced sequentially (i.e, one at a time). Please note that in Fig. 6 (b) although nine holes (where the transmitters were placed) are visible, the side ones in the middle row and middle column have not been used. The center frequency of the transmitters and receivers approximately 40 kHz. From a 38-44 kHz/12 ms chirp signal, according to the procedure described in Sections II, III-A, III-B and III-C, five unique excitation signals were created on a laptop using Matlab for transmission for the conventional, and proposed bandwidth, time and joint optimization methods, respectively. Then, from the laptop, the excitation signals were fed to a measurement-computing USB-1604 data acquisition (DAQ) module [22] connected to a digital-to-analog converter module [22] and finally carried into the transmitters which were programmed to excite simultaneously. The sampling rate of the DAQ was 1 Msample/s and it was also connected to the receivers in order to capture the received signals. In this configuration, the transmitters and receivers were synchronized as they shared a common clock.

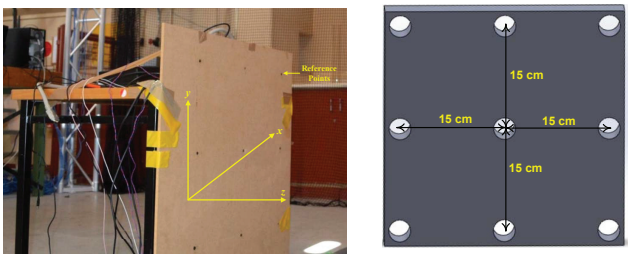


Fig. 6: Experimental setup: (a) configuration of receiver plane; and (b) transmitter plane

To demonstrate the performances of the proposed approaches, using the same signal parameters and setup, the positions of the targets (transmitters) were also calculated by the TDM technique and other three chirp-based multiple-access techniques (set 1, set 2, and set 3) proposed in [17]. The techniques proposed in [17] are considered as state of the art in a chirp-based multiple-access UIPS, as illustrated in [18]. A brief description of these sets is given in Section I. In the experimental setup, to avoid the near-far effect, we ensured that all the receivers received signals of approximately equal strength from the transmitter by confirming that the transmitter

This article has been accepted for publication in a future issue of this journal, but has not been fully edited. Content may change prior to final publication. Citation information: DOI 10.1109/JSEN.2020.3006930, IEEE Sensors Journal



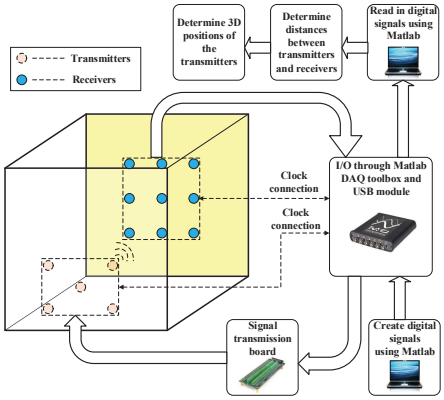


Fig. 7: Illustration of connection diagram between transmission and reception architectures of UIPS

and receiver planes were facing each other and the heights of the central receiver and transmitter were approximately the same. The transmitted and received signals were processed on a laptop to determine their TOFs using cross-correlation and, finally, the positions of the transmitters were computed using spherical multilateration. Note that the setup was the same for every method and each location measurement was repeated 100 times. Detailed descriptions of the distance and position calculations are provided in the following sub-sections.

### A. Distance Estimation

The signal received by a receiver is:

$$r(t) = \sum_{m=1}^{M} A_m \cdot (h_m * s_m)(t - \tau_m) + n(t) \qquad (12)$$

where $M$ = 5 is the number of transmitters, $s_m(t)$ the transmitted signals (which are unique), $A_m$ and $\tau_m$ the amplitude and TOFs, respectively, of the signal to be estimated and $*$ the convolution operator that denotes the filtering response generated by an unknown impulse response ($h_m(t)$) of the ultrasonic channel.

The process for finding the distance information was begun by calculating the TOF between the transmitted and received signals through cross-correlation. The correlation between the $k$th transmitted signal ($s_k(t)$) and received signal $r(t)$ is:

$$c_k(\tau) = (A_k \cdot (h_k * s_k)(t - \tau_k)) \star s_k(t) + \left(\sum_{m \neq k} A_i (h_m * s_i)(t - \tau_m)\right) \star s_k(t) + n(t) \star s_k(t) \qquad (13)$$

The TOF information is embedded in the first term on the right hand-side of equation (13), which can be found from the peak value of $c_k(t)$, whereas the second and third terms represente the MAI and system noise, respectively. Once all the TOF information was available, it was converted into distances ($d_m$) using the common, straightforward law:

$$d_m = v \cdot \tau_m \qquad (14)$$

where $v$ is the speed of the ultrasound which depends on the air temperature ($\vartheta$) and the relationship between them:

$$v = 331.3 + 0.6\vartheta \text{ m/s} \qquad (15)$$

In our system, the measured temperature ($\vartheta$) obtained via a digital thermometer was 23°C . The speed of ultrasound also depends on the humidity which is negligible.

### B. Position Estimation

Using the distance information between the transmitters and receivers, spherical multilateration was used to determine the 3D positions of the targets (transmitters). Multilateration is the process for determining the location coordinates of an unlocalized target $(x, y, z)$ based on knowledge of the $N$ receivers' (i.e., reference points) positions ($(x_n, y_n, 0)$, where $n = 1, 2, \cdots, 9$) and the corresponding measured distances ($d_n$) between the target and receivers. Using the principles of basic geometry, the system of equations can be written as:

$$d_n^2 = (x_n - x)^2 + (y_n - y)^2 + z^2 \qquad (16)$$

This set of quadratic equations is solved by subtracting the last equation from the other ones which gives a set of linear equations. Subsequently, the least squares estimation is used for solving the set.

## VI. Experimental Results

The location of each transmitter was computed for both locations of the transmitter plane with respect to the locations of the reference points using equation (16) (shown in Fig. 8). The mean absolute 3D location errors and $x$,

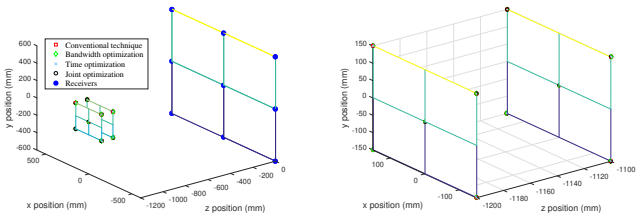


(a) (b)

Fig. 8: Diagram of locations of (a) reference points (receivers) and targets (transmitters) and (b) zoom version of targets (transmitters)

$y$ and $z$ direction errors obtained from the experiments for each transmitter for the TDM, sets 1, 2 (the conventional technique), & 3 of [17] and proposed bandwidth, time, and joint optimization methods are shown in Fig. 9 and Table II with their standard deviations. From the results, it is clear that, for the same environment, the errors of the proposed time and joint optimization methods were much lower than those of the schemes proposed in [17]. Also, the results of the proposed time and joint optimization methods are comparable with those of the TDM technique while the results of the proposed bandwidth optimization were almost the same as those of the conventional scheme (i.e, set 2 of [17]). It has also been noticed that using set 1 of [17], only a maximum of four transmitters was able to localize as it can generate only a maximum of four unique chirp waveforms. Moreover, it can also be observed that the errors in each scheme varied according to the transmitter's index. Comparing Figs. 9(a)

This article has been accepted for publication in a future issue of this journal, but has not been fully edited. Content may change prior to final publication. Citation information: DOI 10.1109/JSEN.2020.3006930, IEEE Sensors Journal



TABLE II: Means and standard deviations of 3D location errors and $x$, $y$, $z$ direction errors (in mm) of conventional technique (i.e, set 2 of [17]), Set 1 of [17], Set 3 of [17] and proposed frequency, time and joint optimization methods

| Methods | Transmitter Index | Mean Error & Standard Deviation of Error | | | |
|---|---|---|---|---|---|
| | | 3D | $x$ | $y$ | $z$ |
| Conventional technique (i.e, set 2 of [17]), Set 1 of [17], Set 3 of [17], Bandwidth optimization, Time optimization & Joint optimization, and TDM | 1 | [12.26, 10.47, 11.90, 11.89, 4.18, 4.07, &2.79] & [6.30, 5.34, 5.98, 6.65, 2.11, 2.04, &1.43] | [7.71, 6.55, 7.48, 7.65, 2.64, 2.52, &1.75] & [5.81, 4.99, 5.53, 5.73, 1.98, 1.89, &1.35] | [7.71, 6.60, 7, 53, 7.25, 2.63, 2.58, &1.76] & [5.87, 4.97, 5.59, 5.51, 1.93, 1.95, &1.30] | [1.34, 1.15, 1.34, 1.37, 0.47, 0.46, &0.32] & [1.02, 0.90, 1.01, 1.04, 0.36, 0.34, &0.24] |
| | 2 | [6.70, 6.26, 6.81, 6.71, 4.72, 4.19, &2.82] & [3.46, 3.19, 3.44, 3.34, 2.35, 2.13, &1.42] | [4.27, 3.86, 4.36, 4.24, 2.99, 2.59, &1.77] & [3.27, 2.98, 3.25, 3.22, 2.23, 1.95, &1.32] | [4.16, 3.97, 4.19, 4.23, 2.87, 2.61, &1.77] & [3.11, 3.00, 3.19, 3.10, 2.22, 2.04, &1.34] | [0.73, 0.71, 0.77, 0.76, 0.51, 0.47, &0.32] & [0.56, 0.53, 0.57, 0.56, 0.38, 0.35, &0.24] |
| | 3 | [4.13, 6.28, 6.78, 6.82, 5.80, 5.10, &2.86] & [2.15, 3.17, 3.57, 3.41, 2.90, 2.54, &1.39] | [2.54, 3.98, 4.42, , 4.35, 3.62, 3.18, &1.83] & [1.94, 2.97, 3.34, 3.24, 2.66, 2.41, 1.33] | [2.65, 3.92, 4.26, 4.21, 3.68, 3.20, &1.77] & [1.96, 2.93, 3.31, 3.20, 2.77, 2.47, &1.34] | [0.46, 0.70, 0.76, 0.77, 0.62, 0.57, &0.32] & [0.35, 0.52, 0.57, 0.58, 0.48, 0.43, &0.24] |
| | 4 | [6.72, 3.61, 3.96, 4.18, 4.72, 4.95, &2.82] & [3.37, 1.81, 2.06, 2.14, 2.36, 2.58, &1.45] | [4.14, 2.31, 2.47, 2.67, 2.93, 3.01, &1.76] & [3.21, 1.71, 1.90, 1.98, 2.22, 2.34, &1.34] | [4.27, 2.23, 2.50, 2.61, 2.99, 3.11, &1.78] & [3.20, 168, 1.90, 1.94, 2.22, 2.42, &1.34] | [0.74, 0.39, 0.45, 0.46, 0.51, 0.55, &0.31] & [0.53, 0.31, 0.33, 0.34, 0.38, 0.41, &0.25] |
| | 5 | [12.24, $N/A$, 6.85, 6.81, 4.19, 4.14, &2.83] & [6.22, $N/A$, 3.56, 3.45, 2.21, 2.07, &1.40] | [7.64, $N/A$, 4.32, 4.35, 2.63, 2.63, &1.75] & [5.81, $N/A$, 3.31, 3.18, 2.06, 1.94, &1.30] | [7.71, $N/A$, 4.28, 4.21, 2.62, 2.58, &1.80] & [5.80, $N/A$, 3.29, 3.12, 2.03, 1.94, &1.34] | [1.31, $N/A$, 0.75, 0.77, 0.46, 0.45, &0.32] & [1.00, $N/A$, 0.57, 0.58, 0.35, 0.35, &0.24] |

and 2(a), it can be seen that the errors are proportional to the width of the auto-correlation. In addition, to compare the

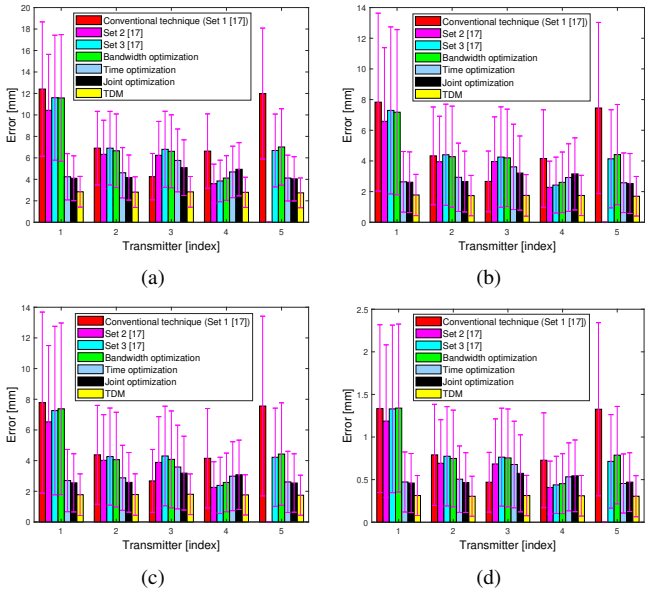


Fig. 9: Means and standard deviations of absolute (a) 3D location errors and (b)-(d) $x$, $y$, $z$ direction errors for conventional and proposed frequency, time and joint optimization methods, respectively

quality parameter between the simulation and experimental results, MLSLRs are presented in Fig. 10 which were obtained from the second experiment. It has been noticed that when the number of transmitters is increased, the MLSLRs are also increased for all techniques. Experimentally, it has been found that when the number of transmitters exceeds five, the results deteriorate more and it was not possible to localize a few of the transmitters. Therefore, the maximum number of emitters that can operate simultaneously was limited to five. For the ease of clarity, the cross-correlation of the received signal (received by the central receiver, considering all five emitters operating simultaneously) with the code pattern of each transmitter is also shown in Fig. 11. Comparing Figs. 4 & 5 and 10 & 11, it can be seen that the MLSLRs and correlation widths obtained from the experiment are slightly higher when compared to the simulation ones. This is because, during the experiment, although it was ensured that there was no multi-path in the environment, this may not happen in a real scenario. Nevertheless, since the experimental results captured those of the correlation analyses, our proposed multiple-access schemes were accurate. Figs. 9(b) to (d) and Table II illustrate

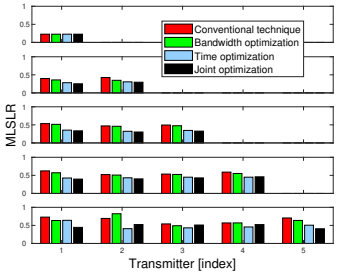


Fig. 10: MLSLR (from experimental results) when all transmitters operating simultaneously

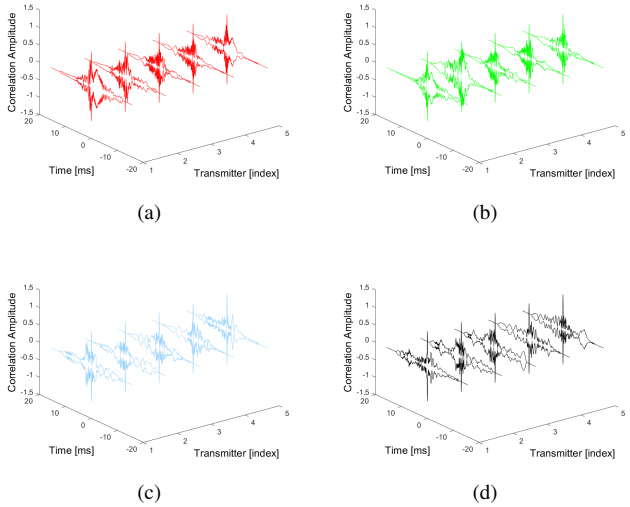


Fig. 11: Cross-correlation of the received signal considering all emitters operating simultaneously (from experimental results): (a) conventional method, (b) proposed bandwidth optimization, (c) proposed time optimization and (d) proposed joint optimization techniques

that the errors in the $x$ & $y$ directions (i.e., lateral ones) were

greater than those in the $z$ direction because we placed all the receivers (i.e., the reference points) on a single plane (i.e., the $z$ plane) which was more accurate and straightforward to instal, particularly in an indoor environment. However, this layout meant that, for positioning, when multilateration was used, the surfaces of the spheres centered at the receivers were approximately parallel when the distances between the reference points and the target was larger than the distance between reference points which is likely to happen. Therefore, more errors were generated in the locations of the intersecting points of the spheres for directions tangential to the surfaces of the spheres (i.e., the $x$ and $y$ directions) than for those perpendicular to the surfaces (i.e., the $z$ direction) [12], a fact known as the dilution of precision (DOP). This kind of error can not only be reduced by using advanced positioning algorithms (e.g., the optimization approach proposed in [12]) but also by installing the reference points at different planes, as described in [1].

## VII. Conclusions and Future Work

In this paper, to enable a multiple-access transmission in a chirp-based UIPS, we proposed three design schemes for waveform diversity, namely, frequency, time and joint optimization ones. Their main advantage was their capability to mitigate the effects of MAI through the design of a unique waveform for each transmitter with an impulse-like auto-correlation and relatively flat cross-correlations to the waveforms transmitted by other transmitters. Their effectiveness was validated through correlation analyses, experiments and comparisons with the conventional scheme. The results showed that the proposed time and joint optimization methods outperformed the proposed bandwidth optimization and conventional methods in terms of range resolution and positioning accuracy. Although the accuracy of the joint optimization technique was slightly higher than that of the time optimization one, its computational complexity was high. Overall, the main disadvantage of the proposed methods is that they are computationally expensive. Nevertheless, as their degrees of freedom are high, they provide an opportunity to increase the number of transmitters in a multiple-access UIPS although some other optimization techniques may be required to search for the optimal parameter set.

It is anticipated that the proposed system can be used for different applications, such as indoor navigation. However, to achieve this, various factors, including the near-far effect, clock synchronization between transmitters and receivers, and the Doppler effect, need to be considered. Although the near-far effect and clock synchronization can be solved by respectively employing the successive interference cancellation algorithm proposed in [6] and timing lock method proposed in [23], the Doppler effect will be considered in the proposed optimization techniques in our future work.

## References


[1] F. J. Álvarez, T. Aguilera, and R. López-Valcarce, "CDMA-based acoustic local positioning system for portable devices with multipath cancellation," *Digital Signal Processing*, vol. 62, no. Supplement C, pp. 38–51, Mar. 2017.

[2] S. Jung, S. Hann, and C. Park, "TDOA-based optical wireless indoor localization using LED ceiling lamps," *IEEE Transactions on Consumer Electronics*, vol. 57, no. 4, pp. 1592–1597, 2011.

[3] J. Ureña, Á. Hernández, J. J. García, J. M. Villadangos, M. C. Pérez, D. Gualda, F. J. Álvarez, and T. Aguilera, "Acoustic local positioning with encoded emission beacons," *Proceedings of the IEEE*, vol. 106, no. 6, pp. 1042–1062, 2018.

[4] M. Hazas and A. Ward, "A novel broadband ultrasonic location system," *UbiComp 2002: Ubiquitous Computing*, pp. 264–280, 2002.

[5] W. Jiang and W. M. Wright, "An indoor airborne ultrasonic wireless communication network," *IEEE transactions on Ultrasonics, Ferroelectrics, and Frequency control*, vol. 65, no. 8, pp. 1452–1459, 2018.

[6] F. Seco, J. C. Prieto, A. R. J. Ruiz, and J. Guevara, "Compensation of multiple access interference effects in CDMA-based acoustic positioning systems," *IEEE Transactions on Instrumentation and Measurement*, vol. 63, no. 10, pp. 2368–2378, Oct. 2014.

[7] L. Segers, J. Tiete, A. Braeken, and A. Touhafi, "Ultrasonic multiple-access ranging system using spread spectrum and MEMS technology for indoor localization," *Sensors*, vol. 14, no. 2, pp. 3172–3187, 2014.

[8] J. R. Gonzalez and C. J. Bleakley, "High–precision robust broadband ultrasonic location and orientation estimation," *IEEE Journal of Selected Topics in Signal Processing*, vol. 3, no. 5, pp. 832–844, 2009.

[9] T. Aguilera, F. Seco, F. J. Álvarez, and A. Jiménez, "Broadband acoustic local positioning system for mobile devices with multiple access interference cancellation," *Measurement*, vol. 116, pp. 483–494, 2018.

[10] M. C. P. Rubio, R. S. Serrano, J. U. Urena, Á. H. Alonso, C. D. Marziani, and F. J. Á. Franco, "Correlator implementation for orthogonal CSS used in an ultrasonic LPS," *IEEE Sensors Journal*, vol. 12, no. 9, pp. 2807–2816, 2012.

[11] D. F. Albuquerque, J. M. N. Vieira, S. I. Lopes, T. Aguilera, and F. J. Álvarez, "High energy OFDM pulse design algorithm for acoustic ToF ranging and localization," in *International Conference on Indoor Positioning and Indoor Navigation (IPIN)*, Oct. 2016, pp. 1–6.

[12] M. O. Khyam, M. J. Alam, A. J. Lambert, M. A . Garratt, and M.R. Pickering, "High-precision ofdm-based multiple ultrasonic transducer positioning using a robust optimization approach," *IEEE Sensors Journal*, vol. 16, no. 13, pp. 5325–5336, 2016.

[13] E. García, J. Ureña, D. Gualda, Á. Hernández, and F. Nombela, "Discrete multitone modulation for ultrasonic indoor positioning systems," in *International Conference on Indoor Positioning and Indoor Navigation (IPIN)*, Oct. 2015.

[14] S. Holm, "Airborne ultrasound data communications: the core of an indoor positioning system," in *IEEE Ultrasonics Symposium, 2005.*, Sep. 2005, vol. 3, pp. 1801–1804.

[15] A. Lindo, E. García, J. Ureña, M. C. Pérez, and Á. Hernández, "Multiband waveform design for an ultrasonic indoor positioning system," *IEEE Sensors Journal*, vol. 15, no. 12, pp. 7190–7199, Dec 2015.

[16] P. Lazik and A. Rowe, "Indoor pseudo-ranging of mobile devices using ultrasonic chirps," in *Proceedings of the 10th ACM Conference on Embedded Network Sensor Systems*, Nov. 2012, pp. 99–112.

[17] M. O. Khyam, L. Xinde, S. S. Ge, and M. R. Pickering, "Multiple access chirp-based ultrasonic positioning," *IEEE Transactions on Instrumentation and Measurement*, Jul. 2017.

[18] S. Murano, C. Pérez-Rubio, D. Gualda, F. J. Álvarez, T. Aguilera, and C. De Marziani, "Evaluation of Zadoff-Chu, Kasami and chirp based encoding schemes for acoustic local positioning systems," *IEEE Transactions on Instrumentation and Measurement*, pp. 1–1, 2019.

[19] H. Shen, S. Machineni, C. Gupta, and A. Papandreou-Suppappola, "Time-varying multichirp rate modulation for multiple access systems," *IEEE Signal Processing Letters*, vol. 11, no. 5, pp. 497–500, May 2004.

[20] C. Gao, K. C. Teh, and A. Liu, "Double-Modulated Frequency Modulation Waveforms for MIMO Radar," *IEEE Geoscience and Remote Sensing Letters*, vol. 13, no. 12, pp. 2024–2028, Dec. 2016.

[21] H. Li, Y. Zhao, Z. Cheng, and D. Feng, "OFDM Chirp Waveform Diversity Design With Correlation Interference Suppression for MIMO Radar," vol. 14, no. 7, pp. 1032–1036, Jul. 2017.

[22] "USB-1604HS-2AO DAQ user's guide, Accessed on Jan. 07, 2020," [Online]. Available: http://www.mccdaq.com/PDFs/Manuals/USB-1604HS-2AO.pdf.

[23] M. M. Saad, C. J. Bleakley, T. Ballal, and S. Dobson, "High–accuracy reference-free ultrasonic location estimation," *IEEE Transactions on Instrumentation and Measurement*, vol. 61, no. 6, pp. 1561–1570, Jun. 2012.

**Mohammad Omar Khyam** received the Ph.D. degree in electrical engineering from the University of New South Wales, Australia, in 2015. He worked as a Postdoctoral Research Fellow with the Advanced Robotics Centre, National University of Singapore, Singapore, from 2016 to 2017, and Center for Bioinspired Science and Technology, Virginia Tech, Blacksburg, VA, USA, from 2018 to 2019. He is currently working as a Lecturer with Central Queensland University, Melbourne, Australia. His current research interests include signal processing, wireless communication, machine learning, and robotics.

**Md. Noor-A-Rahim** received the Ph.D. degree from the Institute for Telecommunications Research, University of South Australia, Adelaide, Australia, in 2015. He was a Postdoctoral Research Fellow with the Centre for Infocomm Technology, Nanyang Technological University, Singapore. He is currently a Senior Postdoctoral Researcher (MSCA Fellow) with the School of Computer Science IT, University College Cork, Cork, Ireland. His research interests include control over wireless networks, intelligent transportation systems, machine learning, signal processing, and DNA-based data storage. Dr. Noor-A-Rahim was the recipient of the Michael Miller Medal from the Institute for Telecommunications Research, University of South Australia, for the most Outstanding Ph.D. Thesis in 2015.

**Xinde Li** (Senior Member, IEEE) received his Ph.D. in Control Theory and Control Engineering, from Department of Control Science and Engineering, Huazhong University of Science and Technology (HUST), Wuhan, China, in 2007. Afterwards, he joined School of Automation, Southeast University, Nanjing, China, where he is currently a Professor and Ph.D. Supervisor. During the period from 2012 to 2013, he was a visiting scholar in School of Interactive Computing, Georgia Institute of Technology. He also worked as a Postdoctoral Research Fellow in Department of Electrical and Computer Engineering, National University of Singapore, from January 2016 to August 2016. His research interests include information fusion, object recognition, computer vision, intelligent robot, and human-robot interaction. He was granted a "Talent of Qing Lan Project" award of Jiangsu province and a "Six Major Top-talent Plan" award of Jiangsu province, China.

**Aruna Jayasuriya** received the B.E. degree in electrical and electronic engineering (first-class honours) from the University of Adelaide, Adelaide, Australia, in 1997 and the PhD in telecommunication engineering from the University of South Australia in 2001. He worked as a senior research fellow with the Institute for Telecommunications Research, University of South Australia, from 20001 to 2010. He is currently the Head of Course, Undergraduate Engineering and a Senior Lecturer with Central Queensland University, Rockhampton, Australia. His current research interests include location prediction using sensor networks, technology-mediated engineering education, and resource allocation in wireless networks.

**Md. Apel Mahmud** (Senior Member, IEEE) received bachelor's degree in electrical engineering with from the Rajshahi University of Engineering and Technology, Rajshahi, Bangladesh, in 2008, and the Ph.D. degree in electrical engineering from the University of New South Wales, Sydney, Australia, in 2012. He is currently working as a Senior Lecturer in electrical renewable energy engineering with Deakin University, Geelong, Australia. He has also worked as a Lecturer in electrical electronic engineering with Deakin University and Swinburne University of Technology, as a Research Fellow with the University of Melbourne, and as a Research Publication Fellow with the University of New South Wales. His research interests include power system stability, control of power systems including renewable energy sources as well as microgrids, energy management for microgrids, energy storage systems, transactive energy (data analytics), and nonlinear control theory. Dr. Mahmud was the recipient of the Best Thesis Award from the University of New South Wales, in 2012.

**Amanullah M. T. Oo** (Senior Member, IEEE) is currently the Dean and the Head of the School of Engineering, Deakin University, Geelong, Australia. He is a Professor of electrical engineering and has made significant research contributions in the area of electrical power engineering and renewable energy, engineering education, and has authored and coauthored more than 250 scholarly articles in the peer reviewed high impact journals, books, and conference proceedings. He has supervised more than 15 Ph.D. students to completion and is currently supervising several Ph.D. students in the area of electrical power engineering and renewable energy engineering. He has led Deakin University 30 million Microgrid research program. His research interests and expertise include microgrid energy storage system integration, smart grid communication, power system stability and control, energy management and efficiency, protection and security of smart grids, sustainable operation and control of microgrids as well as in engineering education. Prof. Maung has been actively working with several international and national professional communities and industries. He is sought worldwide to deliver keynote addresses and presentations at workshops and conferences.

**Shuzhi Sam Ge** (Fellow, IEEE) received the B.Sc. degree from the Beijing University of Aeronautics and Astronautics, Beijing, China, in 1986 and the Ph.D. degree from the Imperial College London, London, U.K., in 1993. He is the Director with the Social Robotics Laboratory of Interactive Digital Media Institute, Singapore and the Centre for Robotics, Chengdu, China, and a Professor with the Department of Electrical and Computer Engineering, National University of Singapore, Singapore, on leave from the School of Computer Science and Engineering, University of Electronic Science and Technology of China, Chengdu. He has co-authored four books and over 300 international journal and conference papers. His current research interests include social robotics, adaptive control, intelligent systems, and artificial intelligence. Dr. Ge is the Editor-in-Chief of the International Journal of Social Robotics (Springer). He has served/been serving as an Associate Editor for a number of flagship journals, including the IEEE TRANSACTIONS ON AUTOMATION CONTROL, the IEEE TRANSACTIONS ON CONTROL SYSTEMS TECHNOLOGY, the IEEE TRANSACTIONS ON NEURAL NETWORKS, and Automatica. He serves as a Book Editor for the Taylor and Francis Automation and Control Engineering Series. He served as the Vice President for Technical Activities from 2009 to 2010 and Membership Activities from 2011 to 2012, and a member of the Board of Governors from 2007 to 2009 at the IEEE Control Systems Society. He is a fellow of the International Federation of Automatic Control, the Institution of Engineering and Technology, and the Society of Automotive Engineering.